

# Use of Biochar from Rice Husk Pyrolysis: Part A: Recovery as an Adsorbent in the Removal of Emerging Compounds

Katherine Herrera, Luisa F. Morales, Natalia A. Tarazona, Roberto Aguado, and Juan F. Saldarriaga\*



Cite This: *ACS Omega* 2022, 7, 7625–7637



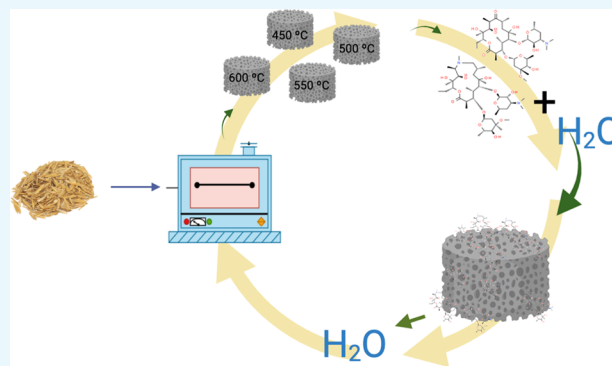
Read Online

ACCESS |

Metrics & More

Article Recommendations

**ABSTRACT:** One of the main products of pyrolysis is char. For the better performance and improvement of its physicochemical properties, it is necessary to make temperature changes. In this study, different temperatures have been tested for the pyrolysis of rice husk, and the biochar obtained from the process went through an evaluation to test its yield in the removal of emerging compounds such as azithromycin (AZT) and erythromycin (ERY). For this, pyrolysis of rice husk has been carried out at temperatures of 450, 500, 550, and 600 °C, and the biochars have been characterized by ultimate analysis and proximate analysis, as well as specific surface area tests. Then, different adsorption tests have been carried out with a 200 mg L<sup>-1</sup> drug (AZT and ERY) solution prepared in the laboratory. All biochars have been found to present removal percentages higher than 95%. Therefore, obtaining biochar from rice husk at any temperature and using it in the removal of high-molecular-weight compounds are quite suitable.



## 1. INTRODUCTION

The annual rice production worldwide is almost 740 million tons. The major producers are China, India, Vietnam, Thailand, the United States, and Pakistan.<sup>1,2</sup> It is estimated that the amount of rice husk can reach 23% of the total mass production, which represents almost 150 million tons per year generated worldwide in rice processing.<sup>3</sup> The use of this biomass as animal food is complex due to its low nutritional content, and on the other hand, its natural degradation is complex because of its silicon content and the abrasive surface.<sup>1</sup> This situation makes it possible to consider the biomass as a new element in the development and use of renewable energy resources and due to its favorable characteristics, specially its low carbon emission and damage to the environment.<sup>1,4</sup> Rice husk has been widely used as a biomass for power energy due to its position as a staple food for more than half of the world's population. The harvest of this grain creates an inexhaustible source of rice husk.<sup>1</sup>

Rice husk can be converted into energy through different processes such as combustion, pyrolysis, or gasification. Of these, pyrolysis is the most promising for rice husks because it has been shown to have high yields in the production of liquids fuel (called bio-oil),<sup>5–9</sup> gases, and solid (biochar).<sup>5,10,11</sup> The bio-oil obtained from pyrolysis has been widely investigated due to its potential use as a second-generation biofuel (after the upgrading process) or as a starting material for chemical compounds.<sup>5,12</sup> The biochar produced comprises typically about 15 wt % of the products, and it is used mainly as a

product for the heat treatment process by combustion or it can be separated. It has also received attention in environmental restoration due to its ability to fix carbon and improve soil fertility.<sup>13,14</sup> At present, the biochar that comes mainly from wood chips, crop stalks, animal carcasses, manure, sludge, and leaves<sup>14–17</sup> is characterized by its high carbon content.

Biochar has been found to have advantageous characteristics, such as a unique pore structure, large specific surface area, complex surface-active functional groups, and stable chemical properties.<sup>14,18</sup> Likewise, it has a high potential for adsorption and removal of pollutants such as heavy metals, immobilization, passivation, and improvement of environmental quality.<sup>14</sup> Biochar has been widely used in studies related to the adsorption of heavy metals in different valence states in water bodies.<sup>14</sup> Compared with traditional activated carbon, the main advantage of biochar is that the raw materials for its production are abundant and low-cost, which can be obtained from agricultural biomass and solid waste, resulting in carbon sequestration and the generation of renewable energy.<sup>15,19</sup> The biochar yields applied in various fields have been reported to

Received: November 3, 2021

Accepted: December 3, 2021

Published: February 25, 2022



be equivalent to or even higher than those of commercial activated carbon and other much more expensive materials such as CNTs and graphene.<sup>15,20–23</sup> Biochar has brought more attention in the field of wastewater treatment as an effective adsorbent of aqueous pollutants, including dyes, organic and phenolic compounds, heavy metals, and active pharmaceutical compounds as anti-inflammatory and antibiotic drugs known for their complex and long-lasting structures.<sup>24–26</sup>

Antibiotics are one of the most used drugs on a daily basis for the prevention, diagnosis, or treatment of diseases in humans and animals.<sup>27</sup> In recent years, antibiotics have attracted increasing interest as an important class of potent pollutants in the environment.<sup>28</sup> After being ingested, a large amount of these and their metabolites are found in the aquatic environment; their complex structures, toxicity, and insufficient treatment in wastewater treatment systems create disturbances in the ecosystems and are potential risks to human health and aquatic life.<sup>24,29</sup> Antibiotic-resistant microorganisms have been recognized as ubiquitous in environments, even those that have never been exposed to antimicrobial agents, and that the environment is an important reservoir of emerging antibiotic-resistant genes.<sup>30</sup> Some authors have reported that low concentrations of drugs in water can affect aquatic organisms and produce oxidative stress, histopathological lesions, as well as genotoxic and immunosuppressive effects, among others.<sup>31</sup>

Among these drugs is azithromycin, which is a macrolide antibiotic and has been reported in treated wastewater from antibiotic-producing companies from  $30 \mu\text{g}\cdot\text{L}^{-1}$  up to  $10.5 \text{ mg}\cdot\text{L}^{-1}$  in the receiving river. A high frequency of bacteria resistant to azithromycin (up to 83%) has also been found in the effluents.<sup>31,33</sup> Managaki et al.<sup>34</sup> found azithromycin in concentrations between 4 and  $448 \text{ ng}\cdot\text{L}^{-1}$  in the urban river of Tamagawa, Japan. In addition, erythromycin, which is also a macrolide,<sup>32</sup> has been found in rivers in concentrations ranging from  $50 \text{ ng}\cdot\text{L}^{-1}$  to  $67.7 \mu\text{g}\cdot\text{L}^{-1}$  in sediments.<sup>33–36</sup> Therefore, the appearance of this class of active pharmaceutical compounds in the aquatic environment has been recognized as one of the emerging issues of environmental chemistry.<sup>37</sup>

Therefore, the use of biochar in the adsorption process of this type of compound is promising for the removal of drugs such as azithromycin and erythromycin from water sources. Biochar has been used in recent years as an adsorbent material for pollutants, but to date, there have been no reports on the study of the obtaining and use of biochar from different temperatures as an adsorbent for emerging pollutants in water. For this reason, the aim of this study is to carry out pyrolysis tests at different temperatures and use the biochar obtained as an adsorbent in the removal of these drugs. This study also aims to determine the working temperature at which a better biochar product can be obtained for the removal of this type of drugs.

## 2. RESULTS AND DISCUSSION

**2.1. Biochar Characterization.** The elemental composition of biochar mainly depends on the physicochemical characteristics of the raw material. In Table 4, it is observed that the composition of the four biochars used in this study is very similar and this varies according to the pyrolysis temperatures and that the changes between these temperatures are minimal. The TGA results shown in Figure 1 show that the thermal decomposition of the organic matrix of the biochar samples at low temperatures is higher, and therefore, this is indicative of adequate volatile matter content (Table 4), which

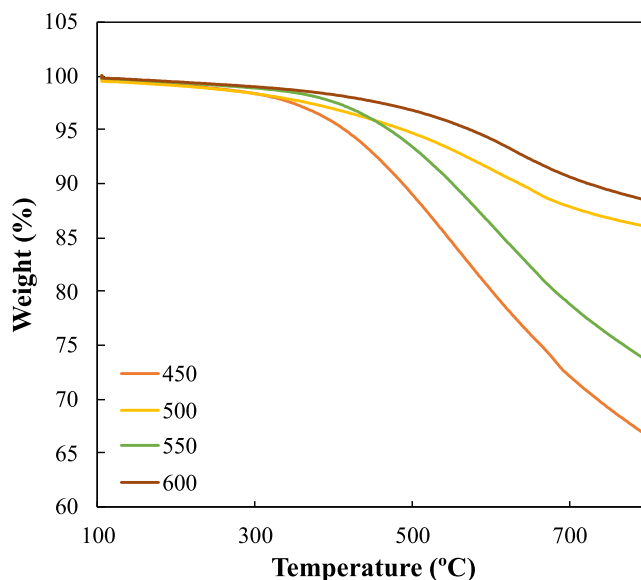


Figure 1. TGA curves for the biochar samples.

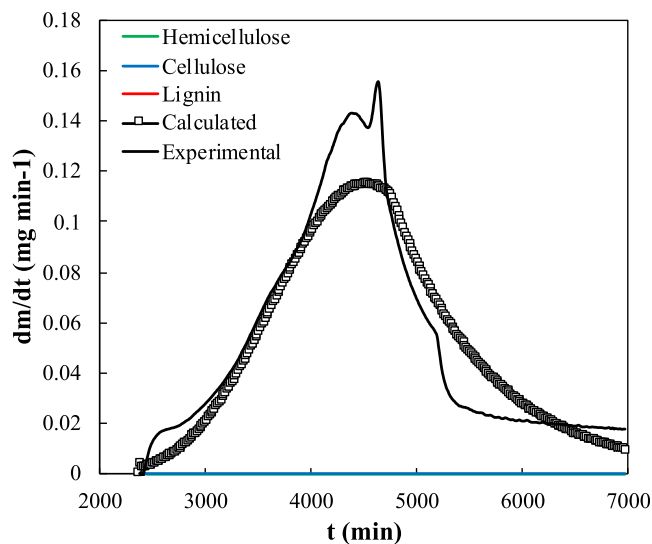


Figure 2. DTG deconvolution for biochar at 500 °C.

Table 1. Specific Surface Area of the Biochar Studied

biochar	$S_{\text{mb}}$ ( $\text{m}^2\cdot\text{g}^{-1}$ )	mean pore size (nm)	micropore volume ( $\text{cm}^3 \text{g}^{-1}$ )
450	$667.84 \pm 0.18$	2.583	0.325
500	$774.83 \pm 0.34$	2.645	0.354
550	$704.19 \pm 0.04$	2.723	0.345
600	$647.89 \pm 0.45$	2.837	0.214

is associated with the pyrolysis temperature during the carbonization process. Therefore, the partial depolymerization of cellulose and lignin from biomass produces low-molecular-weight organic compounds on the surface of the coal, as has been demonstrated by other authors.<sup>38</sup> Figure 2 shows the deconvolution of the three polymeric materials, which shows a good fit despite their degrees of degradation. In the same way, the TGA curves reflect a higher concentration of the inorganic material, with a large mass fraction that remains at 800 °C, which is also due to the characteristics of the rice husk with reported ash contents of up to 24.63%,<sup>39</sup> and this coincides

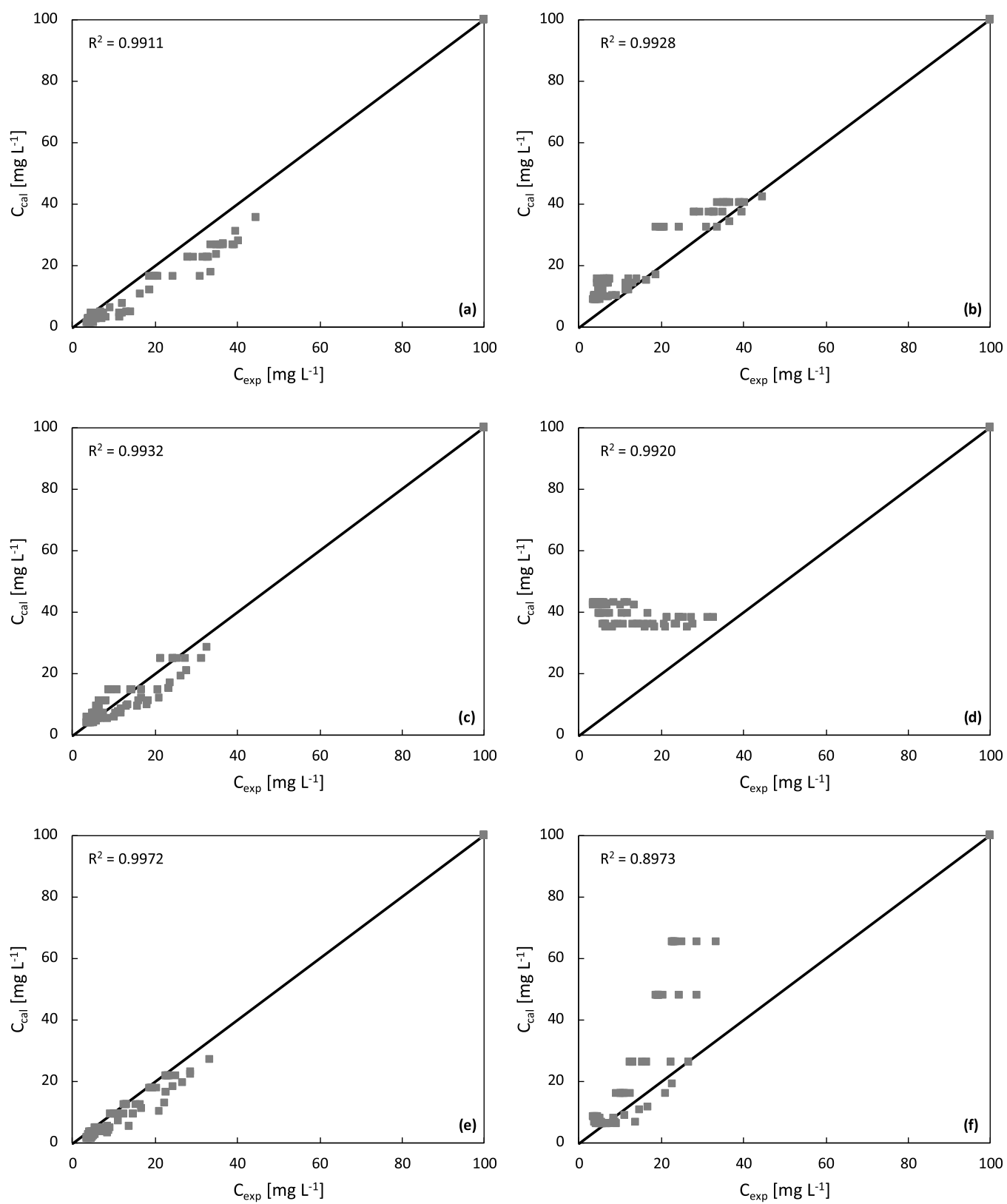
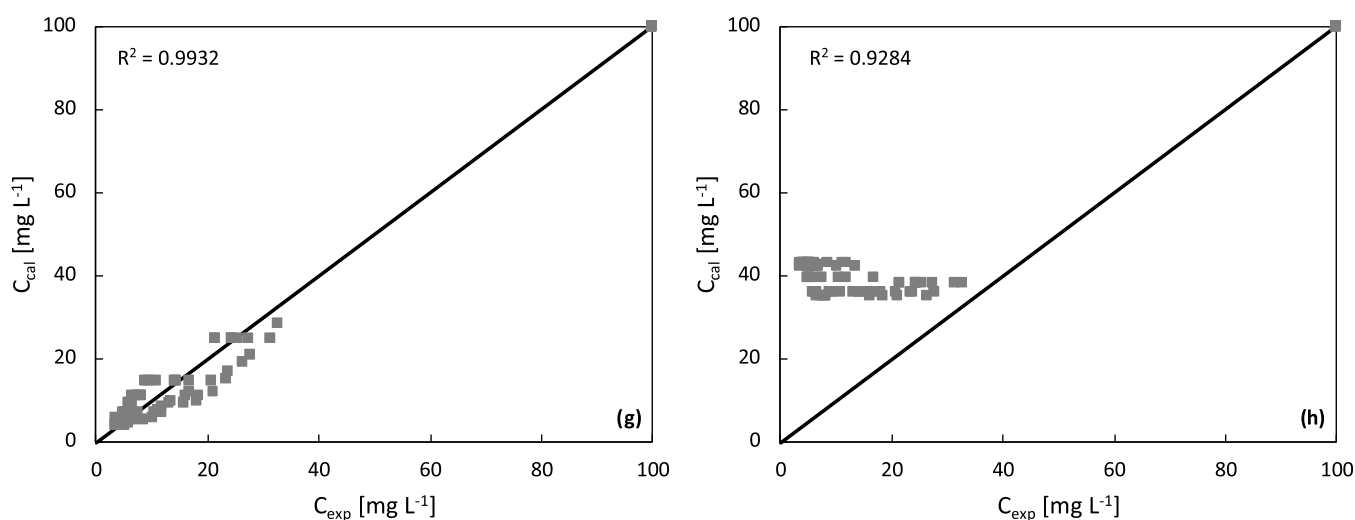


Figure 3. continued



**Figure 3.** Parity charts of the adsorption models tested for AZT. (a) Langmuir isotherm for 450, (b) Freundlich isotherm for 450, (c) Langmuir isotherm for 500, (d) Freundlich isotherm for 500, (e) Langmuir isotherm for 550, (f) Freundlich isotherm for 550, (g) Langmuir isotherm for 600, and (h) Freundlich isotherm for 600.

with the results of this work (Table 4). This concentration is also related to the results of the polymer content on the three main components of the rice husk, and their low content is observed in Table 4. From the results of the polymer content, it is then observed that lignin is much more recalcitrant than hemicellulose and cellulose.<sup>40</sup>

Some studies have reported that rising temperature increases the surface and porosity of a biochar due to the higher degree of carbonization.<sup>19,41</sup> The chemical composition of the surface plays an important role in the adsorption properties of a biochar.<sup>42</sup> Table 1 shows the specific surface areas of the four samples, showing that there are no significant changes in their area, and these are closely related to volatile substances (Table 4) such as cellulose and hemicellulose, and the formation of channel structures during pyrolysis, because there are no significant changes between these samples.<sup>19,43–45</sup> Therefore, it is argued that the release of volatile components during the pyrolysis process facilitates the formation of the vascular bundle structure in the biochar and consequently improves the specific surface area and the pore structure, as observed in Table 1.<sup>46</sup> Some authors have observed a decrease in pore size, the formation of internal pore structures, and an increase in porosity as a result of the release of volatiles during carbonization.<sup>19,44</sup> Similarly, it is evidenced that all of the samples have two types of pores, most of which are micropores with a size of 2 nm; among the samples, it is evidenced that the biochar at 500 °C presents the most abundant pore volume at 2 nm, 0.354 cm<sup>3</sup> g<sup>-1</sup>, which may introduce different properties in applications.<sup>47</sup>

Low-specific-surface-area contents of biochar from rice husk have been reported in the literature, mainly due to the technique used to determine the said area.<sup>17</sup> With the methylene blue technique, the values ranged from 6.96, 71.52 and up to 255.78 m<sup>2</sup>·g<sup>-1</sup>, and the results of this study demonstrate once again that this technique is suitable for measuring the BET area, showing up to 3 times more area than that reported in the literature in the case of the biochar tested.<sup>48–50</sup>

**2.2. Adsorption Isotherms.** Adsorption isotherms are essential to optimize the use of adsorbents, especially biochar, which is an emerging material, low-cost, and easy to acquire.

Biochar has proven in recent years to be an alternative to commercial activated carbons, which have high cost and similar removal efficiencies. The use of adsorption isotherms is important because it describes how adsorbates interact with adsorbents.<sup>51</sup> Several empirical models have been used in the literature to analyze experimental data and describe the equilibrium of the adsorption of heavy metals in biochar.<sup>19</sup> Among the most popular and widely used models are the Langmuir, Freundlich, Langmuir–Freundlich, and Temkin equations. It has been found that in the case of char from biomass, the models that best fit are those of Langmuir and Freundlich.<sup>16,17,19</sup> The results vary widely depending on the properties of the biochar and the compound of interest to be removed.

The behavior observed in this study is similar to those found in other studies.<sup>52</sup> For example, in the literature, zeolites were used for the removal of AZT, reaching high removal levels in the first few minutes of the test and becoming constant over time.<sup>52</sup> The behavior observed with the biochars tested in this study is good and had high  $q_m$  values compared to those found with zeolites in which average values of 8.50 mg·g<sup>-1</sup> were found in removal tests of 10 mg·L<sup>-1</sup> antibiotic.<sup>52</sup>

In Figure 3, the parity graphs are shown, in which the good fit of the data to the Langmuir isotherm is evidenced, demonstrating in this way that the removal follows the behavior of a monolayer. Likewise, it is the same behavior observed in other studies in which it is shown that the compound has a high affinity to solids.<sup>53</sup>

It is observed that the behavior of ERY is like the behavior of AZT (Figure 4), and these fit better on the Langmuir model than on the Freundlich model. This can be observed in the case of AZT (Figure 3) in which the data is stratified and shows that the behavior of the biochars in the removal of both antibiotics is the Langmuir isotherm. This similar behavior may be due to the high molecular weight of both compounds (Table 5). Removal percentages of up to 75% with wood and 66% with coal have been found in other studies, while in this study, removal of more than 95% has been achieved.<sup>54</sup>

ERY adsorption tests with magnetic activated carbon have also been carried out, and the removal process conforms to a Freundlich-type model. Possibly, this behavior is due to the

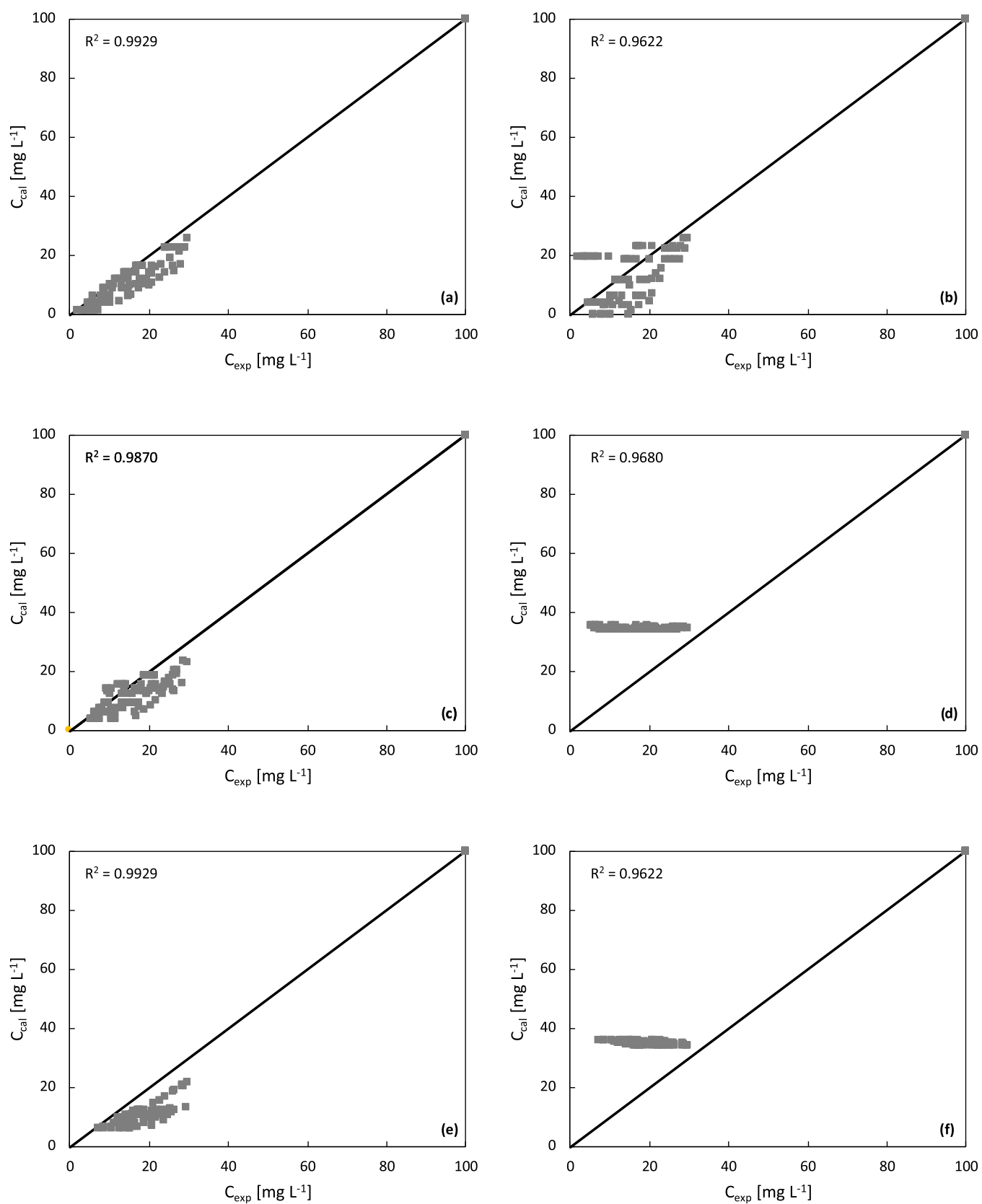
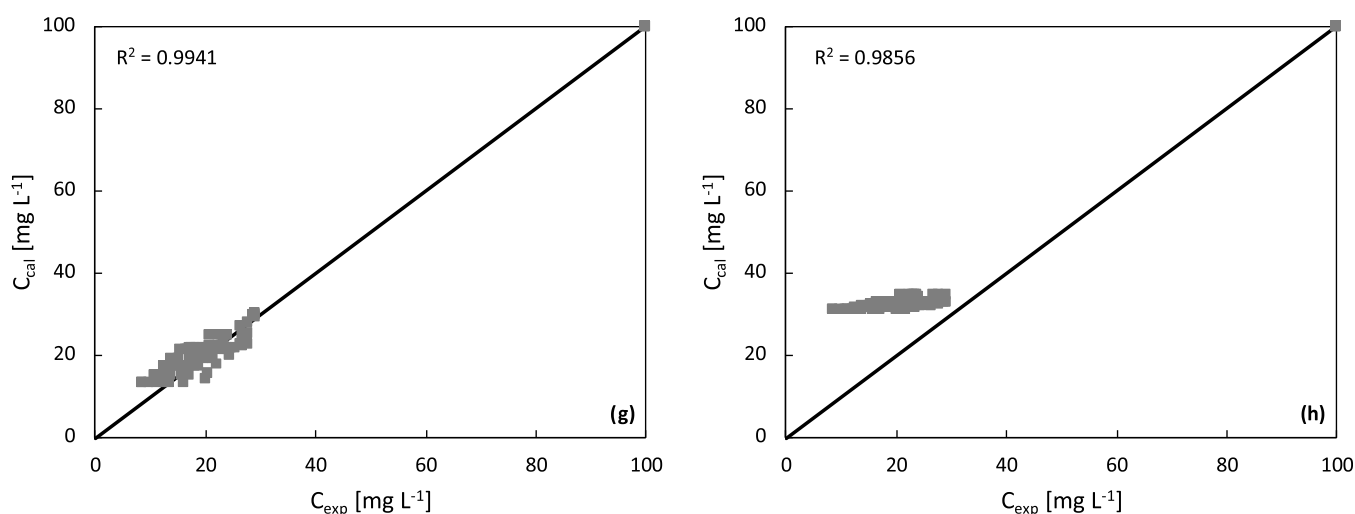


Figure 4. continued



**Figure 4.** Parity charts of the adsorption models tested for ERY. (a) Langmuir isotherm for 450, (b) Freundlich isotherm for 450, (c) Langmuir isotherm for 500, (d) Freundlich isotherm for 500, (e) Langmuir isotherm for 550, (f) Freundlich isotherm for 550, (g) Langmuir isotherm for 600, and (h) Freundlich isotherm for 600.

magnetization of the biochar particles that can influence the affinity to the molecular structure of the compound because in the present study the best model has been achieved with the Langmuir isotherm with  $q_m$  of up to 599.72.<sup>55</sup> Another important factor to consider in the previous differences is the raw material for obtaining the char and its chemical properties.

Figure 5 shows the high removals that can occur with biochar for both antibiotics according to the applied model. These results are interesting because both compounds are macrolide antibiotics with comparable structures and high molecular weights (Table 5). Also, it has been found in other studies that the Langmuir model is the one that best adjusts to the experimental data. It has been observed that in the case of ERY, it is the one that shows the best performance when adjusted.<sup>55</sup> The results show that the Langmuir model correlates satisfactorily with the experimental data, coinciding with other studies for other types of adsorbents used.<sup>56</sup>

These results concord with the kinetic evaluation. Tables 2 and 3 show the balance of the parameters and the mass transfer coefficients calculated for both models evaluated. It is unmistakable that both antibiotics conform to the Langmuir model and that the  $q_m$  is high for both. In the case of AZT, the best  $q_m$  value is obtained with the biochar at 500 °C, while for ERY, this is reached with the biochar at 600 °C. Although the adsorption models fit better for the Langmuir model, it is shown in Table 2 that for the Freundlich case a favorable adsorption occurs at values of  $n$  between 1 and 10, and in the case of this study, all of the values of  $n$  are below the favorable range. Values of  $1/n$  above 1 are said to be indicative of cooperative adsorption.<sup>57</sup> From the results shown in Table 3, it can be seen that the Langmuir isotherm model can satisfactorily correlate the isotherms of the adsorption mechanisms for ERY with the experimental data.<sup>56</sup> It is observed in Table 3 that the  $q_m$  for the four biochars used is quite high, even for the biochar at 600 °C, which reached a value of 599, perhaps as a result of the improvement of the structures and the surface area of the char as the pyrolysis temperature increases.

**2.3. Determination of Functional Groups.** In Figure 6, two FTIRs are shown as examples for both the 600 °C biochar and the 2 g biochar test at 600 °C after the adsorption process.

It is evident that the biochar at 600 °C (Figure 6a) presents two peaks in different ranges: between 1000 and 1100  $\text{cm}^{-1}$  and between 700 and 800  $\text{cm}^{-1}$ . Both peaks can be attributed to the presence of Si–O–Si structures with stretching and curvature vibrations.<sup>58–60</sup> Therefore, these peaks are related to the mineral composition of Si present in the rice husk. However, in Figure 6b, the biochar is observed after the adsorption process. It is evidenced that there is indeed adsorption of the antibiotic, with peaks between the bands 900 and 1700  $\text{cm}^{-1}$  (C–O–C asymmetric stretching) that describe the ERY molecule.<sup>61</sup> Peaks at 1387 are especially observed for C–O groups in ERY, and the peak between 2919 and 3400  $\text{cm}^{-1}$  is assigned to the vibration bonds of OH in ERY.<sup>62</sup>

### 3. EXPERIMENTAL SECTION

**3.1. Experimental Equipment.** The pyrolysis plant used has been described in a previous work (Figure 7).<sup>16</sup> It consists of the following elements: (1) a gas feed system, (2) a flow meter, (3) a temperature controller, (4) a pyrolysis reactor, (5) a cyclone, (6) a gas cooling system, and (7) a liquid collection device. The feeding system was batch.

Nitrogen was used as a fluidizing agent, and its flow rate was controlled by means of a flow meter that allows a feed of 20  $\text{L}\cdot\text{min}^{-1}$ . Before the gas entered the reactor, it was heated in a preheater. The plant was a fixed-bed reactor with dimensions 40 cm wide, 20 cm high, and 63 cm long. To study the composition of the char and its effect on adsorption processes, runs at 450, 500, 550, and 600 °C were carried out. Each experiment was performed on a batch and a feeding of 200  $\text{g}\cdot\text{h}^{-1}$  of rice husk. This process was repeated several times until a suitable sample was obtained to follow out the adsorption experiments. The samples were then sieved, washed several times to eliminate any color interference that the biochar could throw up, and dried.

**3.2. Biochar Characterization.** To study the different types of biochars obtained, and based on previous experience,<sup>8,9,17,39</sup> rice husk was used because of its physicochemical properties. The moisture contents of the four biochars were measured (according to the ISO 589 standard and by means of a halogen moisture analyzer HR83, Mettler Toledo), and the following analyses were done: proximate analysis (in a TA



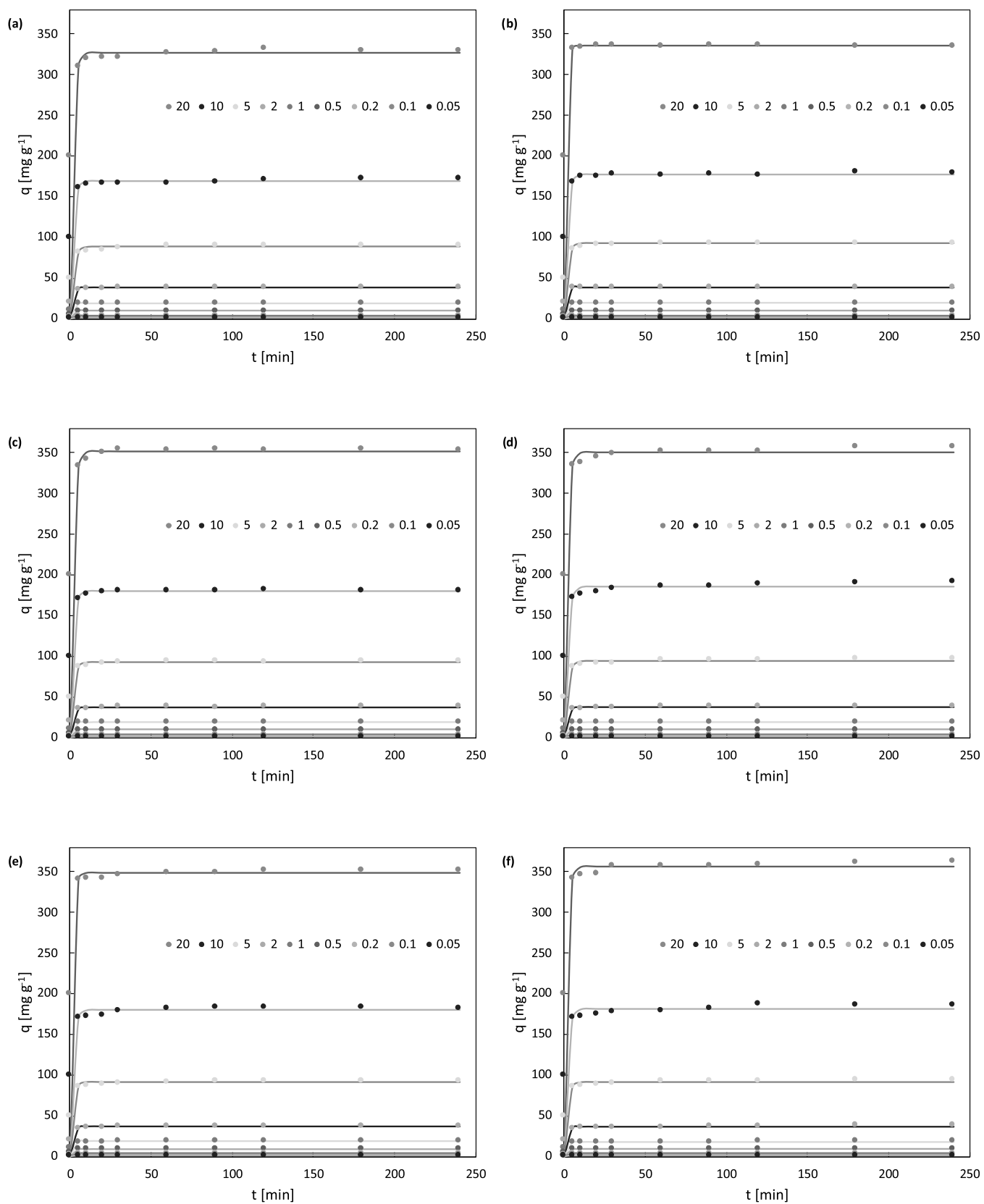
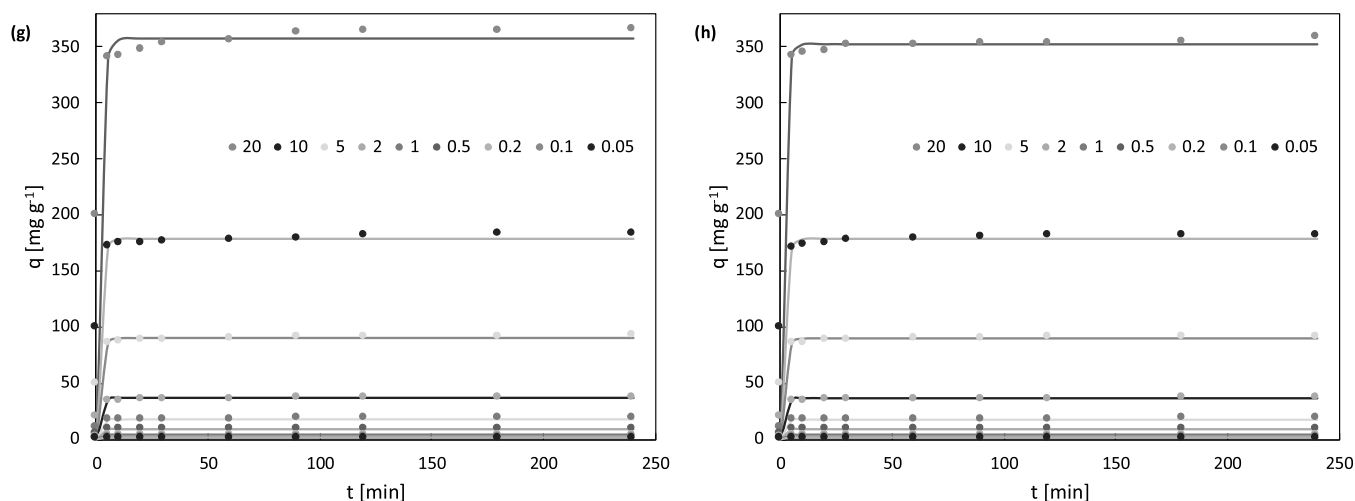


Figure 5. continued



**Figure 5.** AZT and ERY removals by biochar adsorbents for different precipitated masses. Operating conditions: 23 °C, 240 min. (a) AZT-450, (b) AZT-500, (c) AZT-550, (d) AZT-600, (e) ERY-450, (f) ERY-500, (g) ERY-550, and (h) ERY-600.

**Table 2.** Balance Parameters and Mass Transfer Coefficient Calculated for the Models Evaluated for AZT

model	parameter	biochar			
		450	500	550	600
Langmuir	$k_1 a \rho_b$ ( $\text{min}^{-1}$ )	0.830	0.806	0.839	0.866
	OF	0.991	0.998	0.997	0.993
	$k_L$ ( $\text{L}\cdot\text{m}^{-2}\cdot\text{min}^{-1}$ )	0.0163	0.0171	0.0161	0.0182
	$q_m$ ( $\text{mg}\cdot\text{g}^{-1}$ )	494.67	612.22	603.63	499.24
Freundlich	$K_F$	0.825	0.847	0.925	0.989
	$n$	0.686	0.645	0.728	0.842
	OF	0.993	0.998	0.897	0.928

**Table 3.** Balance Parameters and Mass Transfer Coefficient Calculated for the Models Evaluated for ERY

model	parameter	biochar			
		450	500	550	600
Langmuir	$k_1 a \rho_b$ ( $\text{min}^{-1}$ )	0.631	0.563	0.485	0.577
	OF	0.993	0.987	0.991	0.994
	$k_L$ ( $\text{L}\cdot\text{m}^{-2}\cdot\text{min}^{-1}$ )	0.0161	0.0160	0.0175	0.0075
	$q_m$ ( $\text{mg}\cdot\text{g}^{-1}$ )	502.84	496.73	525.04	599.72
Freundlich	$K_F$	0.724	0.786	0.795	0.939
	$n$	0.570	0.772	0.777	0.790
	OF	0.962	0.968	0.975	0.986

Instruments Discovery 5500 TGA according to the ASTM D5142 standard), ultimate analysis (Vario–Macro of Elemental, according to the ASTM D5373 and ISO 19579 standards), and HHV (Parr 6200 isoperibolic bomb calorimeter following the ASTM D5865 standard). The contents of the three natural polymers that make up the biomass were determined according to the methodology proposed by different authors,<sup>6,7,39</sup> by means of a deconvolution of the DTG curves obtained in the same equipment used for proximate analysis (TGA Discovery 5500 TA Instruments). For the determination of the three components, an algorithm was developed in Scilab 6.0.1 that solves the ordinary differential equations of a kinetic model that considers the three independent parallel reactions corresponding to the degradation of each component.<sup>6,7,11,39</sup> Similarly, the algorithm uses a direct search optimization established by Nelder–Mead to find the values of the best fit for the kinetic model (frequency factors and activation energies) and for the

contents of two of the three polymers. The objective function to be minimized is the sum of the squared differences between the experimental TGA values and those calculated by the model. All of the physicochemical characteristics of the biochar used in this study are shown in Table 4, where wt % d.b. represents the weight percent on a dry basis and wt % w.b. represents the weight percent on a wet basis.

It is observed that the moisture content of the four biochars is quite low. The fixed carbon in all biochars ranged between 48.65% and 54.59%. High volatile matter content and low ash content indicate significant conversion to pyrogenic vapor during heat treatment and low biochar yield.<sup>63,64</sup> Higher volatile biomass is undesirable for bio-oil production together with biochar.<sup>63</sup> Table 1 shows the carbon, hydrogen, sulfur, hydrogen and nitrogen composition of both the raw material and all the biochars obtained, noting that the carbon content increases considerably with respect to the raw material. The contents of C, H, N, S, and O of the biochar were studied, and



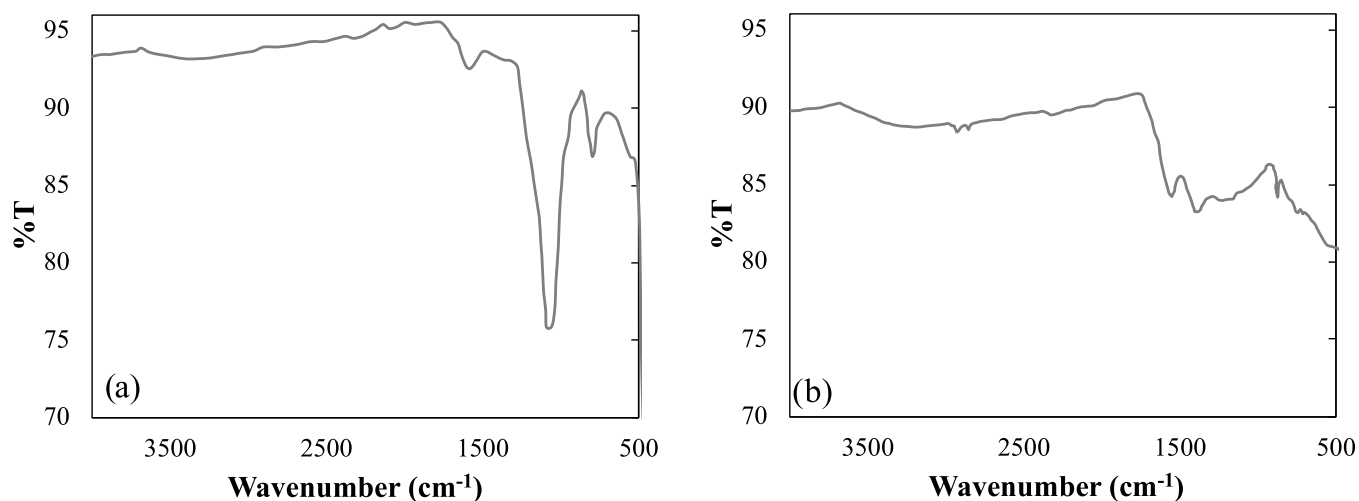


Figure 6. Fourier transform infrared (FTIR) spectra. (a) Biochar 600 °C without adsorption, (b) biochar 600 °C with 2 g after adsorption.

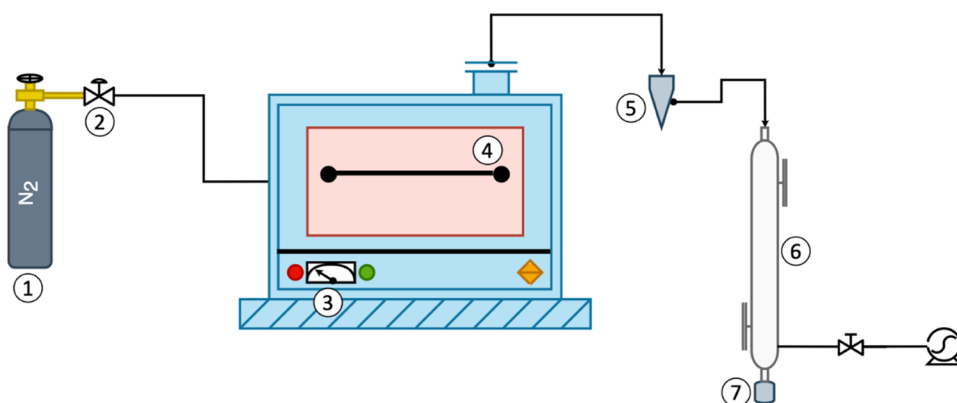


Figure 7. Schematic diagram of the pyrolysis plant.

Table 4. Physical–Chemical Characteristics of the Biochar Used

parameter	biochar				
	rice husk	450	500	550	600
Ultimate Analysis					
nitrogen (wt % d.b.)	0.70	0.59	0.62	0.50	0.48
carbon (wt % d.b.)	31.60	63.90	64.20	65.60	69.3
sulfur (wt % d.b.)	0.01	0.28	0.31	0.20	0.27
hydrogen (wt % d.b.)	4.35	1.52	1.25	1.30	1.28
oxygen (wt % d.b.)	47.37	9.71	8.62	7.40	6.67
Proximate Analysis					
moisture (wt % w.b.)	8.40	0.54	0.32	0.24	0.23
volatile matter (wt % d.b.)	65.33	22.06	24.09	24.84	27.00
fixed carbon (wt % d.b.)	10.04	54.59	52.45	51.57	48.65
ash (wt % d.b.)	24.63	22.81	23.14	23.35	24.12
HHV (MJ/kg)	13.76	11.95	10.27	14.03	15.12
Proposed Polymer Source					
hemicellulose (wt % d.b.)	15.00	0.00	0.00	0.00	0.00
cellulose (wt % d.b.)	30.80	4.26	0.00	0.00	0.00
lignin (wt % d.b.)	26.40	25.32	15.56	9.64	3.23

it was possible to observe that the C content was high and the contents of N and S were quite low. Similarly, it can be seen that at a temperature of 450 °C there is a small amount of cellulose on the polymer content and a large amount of lignin,

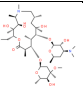
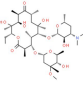
but all of the hemicellulose had already been consumed. For temperatures of 500, 550, and 600 °C, only lignin was observed in its content, and this is in accordance with research in which it is argued that after 500 °C hemicellulose and cellulose completely degraded.<sup>6,7,11,39</sup>

Likewise, the surface area of each of the biochars obtained was evaluated with methylene blue dye, which is widely used for mineral clay. In recent years, it has been used for biochar because its amorphous and asymmetric compositions do not show good results, as seen from BET isotherms.<sup>65</sup> Therefore, methylene blue adsorption measurements are used for a more accurate determination of the surface area for liquid adsorption applications.<sup>38,65</sup> In the same way, and to evaluate the pore size, a BET area analysis was carried out on an AutoChem II 2920 equipment (Micromeritics).

To determine functional groups, FTIR analysis was performed using an infrared spectrometer (PerkinElmer, model spectrum Two V10.4.2) equipped with an attenuated total reflection (ATR) accessory (PerkinElmer), operating in the spectral range of 4000–400  $\text{cm}^{-1}$  with a resolution of 4  $\text{cm}^{-1}$ .

**3.3. Drug Adsorption Capacity Procedure.** Two pharmaceutical compounds (AZT and ERY) were chosen for the adsorption process due to their wide use and sale without prescription. For this study, the water to be treated was contaminated and brought to a maximum concentration of 100  $\text{mg L}^{-1}$  for both AZT and ERY<sup>66</sup> (Table 5) through a

Table 5. Characteristics of the Investigated Antibiotics<sup>a,b,c</sup>

Antibiotic	Structure <sup>a</sup>	CAS N <sup>o</sup>	MW (Da)	pK <sub>a</sub> <sup>b</sup>	Water Solubility (mg L <sup>-1</sup> ) <sup>b</sup>	Log K <sub>ow</sub> <sup>b</sup>	Molar volume (cm <sup>3</sup> ) <sup>a</sup>
AZT		83905-	748.98	8.74	2.37 <sup>c</sup>	4.02	632.7 ±
		01-5					5
ERY		114-07-	733.93	8.90	4.20 <sup>c</sup>	3.06	607.2 ±
		08					5

<sup>a</sup>www.chemspider.com/. <sup>b</sup>www.pubchem.ncbi.nlm.nih.gov/. <sup>c</sup>H<sub>2</sub>O, 25 °C.

sonication process for 1 h. The adsorption tests were carried out for all of the temperatures at which the rice husk biochars were obtained. The above tests were performed to observe which of the four biochars have a better behavior in the process of removal of these types of compounds in contaminated water.

For the adsorption tests, eight groups of carbon samples were prepared, each with ten different weights in the range of 0–20 g, for a total of 80 samples deposited in amber bottles with a volume of 100 mL of contaminated water in each. The flasks were then placed in the Model SIF 3000 Shaker (MAX QTM, Chandler) at room temperature and 120 rpm.

For the removal reading, 5 mL was taken from each bottle in test tubes, and they were subjected to a rapid centrifugation process (1200 rpm) for 1 min. After this, the content of each tube was filtered through qualitative paper to separate the liquid phase from any remaining solid carbon particles. The absorbance was measured in the spectrophotometer, and with each value obtained, the concentration removal was calculated.

The calibration of the tests was performed according to ASTM D3860-98.<sup>66</sup> A Genesys UV Thermo spectrophotometer (Thermo Fisher Scientific) was used to measure different wavelengths to the test solutions at a concentration of 200 mg·L<sup>-1</sup>. For AZT, the wavelength was 222 nm, and for ERY, it was 200 nm.

For calibration, 10 drug solutions were prepared with water at concentrations of 5–400 mg·L<sup>-1</sup> of AZT and ERY, measuring the value of absorbance and keeping the calculated wavelength value constant. A curve was made where each of the concentrations and their absorbances were related. For AZT, a slope of 0.0053, an intercept of −0.0159, and an R<sup>2</sup> of 0.99943 were obtained. In the case of ERY, a slope of 0.0035, an intercept of −0.0019, and an R<sup>2</sup> of 0.9979 were obtained.

**3.4. Adsorption Model.** Previous studies of the investigation group evaluated the adsorption of different emerging pollutants, and these followed the Langmuir model (eq 1) and the Freundlich model (eq 2) that have been widely accepted in the literature<sup>67</sup>

$$q_e = \frac{Q_{\max}^0 K_L C_e}{1 + K_L C_e} \quad (1)$$

$$q_e = K_F C_e^n \quad (2)$$

where  $Q_{\max}^0$  (mg·g<sup>-1</sup>) is the maximum saturated monolayer adsorption capacity of an adsorbent,  $q_e$  (mg·g<sup>-1</sup>) is the amount of adsorbate uptake at equilibrium,  $K_L$  (L·mg<sup>-1</sup>) is the constant related to the affinity between an adsorbent and adsorbate,  $C_e$  (mg·L<sup>-1</sup>) is the adsorbate concentration at equilibrium,  $K_F$  (mg·g<sup>-1</sup>)/(mg·L<sup>-1</sup>) is the Freundlich constant, and  $n$  is the Freundlich intensity parameter, which indicates the magnitude of the adsorption driving.<sup>67–69</sup>

According to different authors, on the one hand, the Langmuir model assumes that there is a fixed number of accessible sites available on the surface of the adsorbent and that once the adsorbate occupies a site, no more adsorptions can occur at that site. On the other hand, the Freundlich model cannot describe the linearity relationship at very low concentrations or the saturation effect at very high concentrations.<sup>16,17,67,70</sup>

Similarly, the adsorption kinetics, which represents the dynamics of the adsorption process, has been analyzed by the mass balance of the adsorbate between the liquid and the solid and is described as follows

$$q_e = q_t(1 - e^{-k_1 t}) \quad (3)$$

$$\frac{dc}{dt} = \frac{-k_1 \alpha S(c - c_e)}{L} \quad (4)$$

$$\frac{dc}{dt} = k_L \alpha (c - c_e) \quad (5)$$

where  $q_e$  and  $q_t$  are the amounts of adsorbate uptake per mass of adsorbent at equilibrium and at any time  $t$  (min), respectively;  $k_1$  (min<sup>-1</sup>) is the rate constant of the pseudo-first-order kinetic equation (PFO);  $k_L$  (L·m<sup>-2</sup>·min<sup>-1</sup>) is the mass transfer coefficient;  $a$  (m<sup>2</sup>·g<sup>-1</sup>) is the external surface area of the adsorbent;  $L$  is the volume of the drug solution, and  $\rho_b$  (kg·m<sup>-3</sup>) is the adsorbent bed density.  $k_1 a \rho_b$  represents the rate constant of the pseudo-first-order kinetic model.

For the calculation of the equilibrium parameters of the Freundlich and Langmuir models eqs 1 and 2, previous procedures published by the research group have been followed.<sup>16,17,70</sup> To obtain the data, these were optimized by minimizing an objective function, OF, defined as the sum of squares of the differences between the values of the adsorbate concentration in the liquid phase measured experimentally,  $c_{\text{exp}}$ , and the values calculated by the model,  $c_{\text{cal}}$ . For this, a

calculation algorithm was implemented in MATLAB, which uses the *ode* subroutine to solve the mass balance equations, eqs 1 and 2, and the *fminsearch* subroutine, which calculates the unrestricted minimum of the objective function, based on the Nelder–Mead algorithm.

#### 4. CONCLUSIONS

With the results of this study, progress is made in obtaining materials that can be used as adsorbents for the removal of emerging pollutants, such as macrolide antibiotics, characterized by their high molecular weight and difficulty to remove from sources of waters. It has been found that the biochars obtained from the pyrolysis process all present high removal efficiencies for both pollutants. As has been shown with the applied isotherm models and the FTIR analysis, the drugs have been removed in a large proportion, completely changing the structure of the biochar. With this, it is verified that the rice husk biochar is suitable to be used as an adsorbent for emerging compounds such as AZT and ERY, antibiotics widely used commercially and freely available in countries such as Colombia. For the two antibiotics, the biochars obtained at 450 and 500 °C present better removal conditions and are therefore the most economically appropriate within the pyrolysis process because it is not necessary to use high energies to obtain them due to the high temperatures that would be necessary for the other biochar. It is observed that in the case of AZT the best removal option is with a biochar obtained at 500 °C, while in the case of ERY the biochar obtained at 600 °C is the best. The four biochars present removals above 95% for both antibiotics, and their reported  $q_m$  values are all very high, with the biochars obtained at 450 and 500 °C being the ones that present the best removals. However, it is important to point out that the costs of the pyrolysis process will rise as the temperatures get higher due to the energy consumption that is implicit.

#### ■ AUTHOR INFORMATION

##### Corresponding Author

Juan F. Saldarriaga – Department of Civil and Environmental Engineering, Universidad de Los Andes, 111711 Bogotá, Colombia; [orcid.org/0000-0002-2902-2305](https://orcid.org/0000-0002-2902-2305); Email: [jf.saldarriaga@uniandes.edu.co](mailto:jf.saldarriaga@uniandes.edu.co), [juanfelorza@gmail.com](mailto:juanfelorza@gmail.com)

##### Authors

Katherine Herrera – Department of Civil and Environmental Engineering, Universidad de Los Andes, 111711 Bogotá, Colombia

Luisa F. Morales – Department of Civil and Environmental Engineering, Universidad de Los Andes, 111711 Bogotá, Colombia

Natalia A. Tarazona – Institute of Active Polymers, Helmholtz-Zentrum Hereon, 14513 Teltow, Germany

Roberto Aguado – Department of Chemical Engineering, University of the Basque Country, 48080 Bilbao, Spain; [orcid.org/0000-0001-8743-5696](https://orcid.org/0000-0001-8743-5696)

Complete contact information is available at: <https://pubs.acs.org/10.1021/acsomega.1c06147>

##### Author Contributions

K.H.: Investigation, formal analysis, writing—original draft. L.F.M.: Investigations, formal analysis. N.A.T.: Conceptualization, supervision, validation, writing—review & editing. R.A.:

Conceptualization, validation, formal analysis, writing—review & editing. J.F.S.: Conceptualization, writing—original, writing—review & editing, supervision, validation, resources, funding acquisition, project administration. The manuscript was written through contributions of all authors. All authors have read and given approval to the final version of the manuscript.

##### Notes

The authors declare no competing financial interest. All data generated or analyzed during this study were examined by our group and certified several times.

#### ■ ACKNOWLEDGMENTS

This work was carried out with financial support from the Department of Civil and Environmental Engineering at Universidad de los Andes. This publication was partially made possible by the call for proposals CI-0120: “Publish your new knowledge or expose your new creations” from the Office Vice President for Research and Creation at Universidad de los Andes.

#### ■ NOMENCLATURE

$\alpha$	external surface area of the adsorbent ( $\text{m}^2 \text{g}^{-1}$ )
$\rho_b$	adsorbent bed density ( $\text{kg m}^{-3}$ )
$c_{\text{cal}}$	values calculated by the model
$C_e$	adsorbate concentration at equilibrium ( $\text{mg l}^{-1}$ )
$c_{\text{exp}}$	phase measured experimentally
$C_i$	concentration of the aqueous phase at time $i$ ( $\text{mg L}^{-1}$ )
$C_{\text{sludge}}$	initial sludge concentration (wt %)
$i$	sampling time
$k_1$	rate constant of the PFO equation ( $\text{min}^{-1}$ )
$K_F$	Freundlich constant, ( $\text{mg g}^{-1}$ )/( $\text{mg L}^{-1}$ )
$K_L$	constant related to the affinity between an adsorbent and an adsorbate ( $\text{L mg}^{-1}$ )
$k_L$	mass transfer coefficient ( $\text{L m}^{-2} \text{min}^{-1}$ )
$K_L \alpha \rho_b$	rate constant of the pseudo-first-order kinetic (PFO) model
$L$	volume of the drug solution (l)
$m_{\text{sludge}}$	initial sludge mass (g)
$n$	Freundlich intensity parameter (dimensionless)
$Q_{\text{max}}^0$	maximum saturated monolayer adsorption capacity of an adsorbent ( $\text{mg g}^{-1}$ )
$q_e, q_t$	amounts of adsorbate uptake per mass of adsorbent at equilibrium
$S_{\text{BET}}$	BET specific surface area ( $\text{m}^2 \text{g}^{-1}$ )
$t$	time (min)

#### ■ REFERENCES

- (1) Chen, R.; Congress, S. S. C.; Cai, G.; Duan, W.; Liu, S. Sustainable Utilization of Biomass Waste-Rice Husk Ash as a New Solidified Material of Soil in Geotechnical Engineering: A Review. *Constr. Build. Mater.* **2021**, *292*, No. 123219.
- (2) Lazzari, E.; Polidoro, A.; dos, S.; Onorevoli, B.; Schena, T.; Silva, A. N.; Scapin, E.; Jacques, R. A.; Caramão, E. B. Production of Rice Husk Bio-Oil and Comprehensive Characterization (Qualitative and Quantitative) by HPLC/PDA and GC × GC/QMS. *Renew. Energy* **2019**, *135*, 554–565.
- (3) Sandhu, R. K.; Siddique, R. Influence of Rice Husk Ash (RHA) on the Properties of Self-Compacting Concrete: A Review. *Constr. Build. Mater.* **2017**, *153*, 751–764.
- (4) Thomas, B. S. Green Concrete Partially Comprised of Rice Husk Ash as a Supplementary Cementitious Material – A Comprehensive Review. *Renewable Sustainable Energy Rev.* **2018**, *82*, 3913–3923.

- (5) Li, Z.; Zhong, Z.; Zhang, B.; Wang, W.; Seufitelli, G. V. S.; Resende, F. L. P. Catalytic Fast Co-Pyrolysis of Waste Greenhouse Plastic Films and Rice Husk Using Hierarchical Micro-Mesoporous Composite Molecular Sieve. *Waste Manag.* **2020**, *102*, 561–568.
- (6) Rodríguez, F.; Cruz, Y.; Estiati, I.; Saldarriaga, J. F. Kinetic Study of Corn and Sugarcane Waste Oxidative Pyrolysis. *Energies* **2019**, *12*, No. 4594.
- (7) Osorio-Castiblanco, D. F.; Peyre, G.; Saldarriaga, J. F. Physicochemical Analysis and Essential Oils Extraction of the Gorse (*Ulex Europaeus*) and French Broom (*Genista Monspessulana*), Two Highly Invasive Species in the Colombian Andes. *Sustainability* **2020**, *12*, No. 57.
- (8) Saldarriaga, J. F.; Aguado, R.; Atxutegi, A.; Bilbao, J.; Olazar, M. Kinetic Modelling of Pine Sawdust Combustion in a Conical Spouted Bed Reactor. *Fuel* **2018**, *227*, 256–266.
- (9) Aguado, R.; Saldarriaga, J. F.; Atxutegi, A.; Bilbao, J.; Olazar, M. Influence of the Kinetic Scheme and Heat Balance on the Modelling of Biomass Combustion in a Conical Spouted Bed. *Energy* **2019**, *175*, 758–767.
- (10) Bridgwater, A. V. Review of Fast Pyrolysis of Biomass and Product Upgrading. *Biomass Bioenergy* **2012**, *38*, 68–94.
- (11) Saldarriaga, J. F.; Patiño, J. L.; Lizarazo, M. J. Kinetic Study of Spiny Retamo (*Ulex Euroioeus* L.) Waste Oxidative Pyrolysis. *Chem. Eng. Trans.* **2018**, *70*, 1249–1254.
- (12) Czernik, S.; Bridgwater, A. V. Overview of Applications of Biomass Fast Pyrolysis Oil. *Energy Fuels* **2004**, *18*, 590–598.
- (13) Laird, D. A.; Fleming, P.; Davis, D. D.; Horton, R.; Wang, B.; Karlen, D. L. Impact of Biochar Amendments on the Quality of a Typical Midwestern Agricultural Soil. *Geoderma* **2010**, *158*, 443–449.
- (14) Qiu, B.; Tao, X.; Wang, H.; Li, W.; Ding, X.; Chu, H. Biochar as a Low-Cost Adsorbent for Aqueous Heavy Metal Removal: A Review. *J. Anal. Appl. Pyrolysis* **2021**, *155*, No. 105081.
- (15) Tan, X.; Liu, S.; Liu, Y.; Gu, Y.; Zeng, G.; Hu, X.; Wang, X.; Liu, S.; Jiang, L. Biochar as Potential Sustainable Precursors for Activated Carbon Production: Multiple Applications in Environmental Protection and Energy Storage. *Bioresour. Technol.* **2017**, *227*, 359–372.
- (16) Rodríguez, F.; Montoya-Ruiz, C.; Estiati, I.; Saldarriaga, J. F. Removal of Drugs in Polluted Waters with Char Obtained by Pyrolysis of Hair Waste from the Tannery Process. *ACS Omega* **2020**, *5*, 24389–24402.
- (17) Saldarriaga, J. F.; Montoya, N. A.; Estiati, I.; Aguayo, A. T.; Aguado, R.; Olazar, M. Unburned Material from Biomass Combustion as Low-Cost Adsorbent for Amoxicillin Removal from Wastewater. *J. Clean. Prod.* **2021**, *284*, No. 124732.
- (18) Xiao, F.; Bedane, A. H.; Mallula, S.; Sasi, P. C.; Alinezhad, A.; Soli, D.; Hagen, Z. M.; Mann, M. D. Production of Granular Activated Carbon by Thermal Air Oxidation of Biomass Charcoal/Biochar for Water Treatment in Rural Communities: A Mechanistic Investigation. *Chem. Eng. J. Adv.* **2020**, *4*, No. 100035.
- (19) Tan, X.; Liu, Y.; Zeng, G.; Wang, X.; Hu, X.; Gu, Y.; Yang, Z. Application of Biochar for the Removal of Pollutants from Aqueous Solutions. *Chemosphere* **2015**, *125*, 70–85.
- (20) Angin, D.; Köse, T. E.; Selengil, U. Production and Characterization of Activated Carbon Prepared from Safflower Seed Cake Biochar and Its Ability to Absorb Reactive Dyestuff. *Appl. Surf. Sci.* **2013**, *280*, 705–710.
- (21) Dehkhoda, A. M.; Ellis, N.; Gyenge, E. Electrosorption on Activated Biochar: Effect of Thermo-Chemical Activation Treatment on the Electric Double Layer Capacitance. *J. Appl. Electrochem.* **2014**, *44*, 141–157.
- (22) Jung, C.; Phal, N.; Oh, J.; Chu, K. H.; Jang, M.; Yoon, Y. Removal of Humic and Tannic Acids by Adsorption–Coagulation Combined Systems with Activated Biochar. *J. Hazard. Mater.* **2015**, *300*, 808–814.
- (23) Nguyen, M.-V.; Lee, B.-K. A Novel Removal of CO<sub>2</sub> Using Nitrogen Doped Biochar Beads as a Green Adsorbent. *Process Saf. Environ. Prot.* **2016**, *104*, 490–498.
- (24) Chakhtouna, H.; Benzeid, H.; Zari, N.; Qaiss, A. elkacem.; Bouhfid, R. Functional CoFe<sub>2</sub>O<sub>4</sub>-modified Biochar Derived from Banana Pseudostem as an Efficient Adsorbent for the Removal of Amoxicillin from Water. *Sep. Purif. Technol.* **2021**, *266*, No. 118592.
- (25) Akkaya Saygılı, G.; Saygılı, H.; Koyuncu, F.; Güzel, F. Development and Physicochemical Characterization of a New Magnetic Nanocomposite as an Economic Antibiotic Remover. *Process Saf. Environ. Prot.* **2015**, *94*, 441–451.
- (26) Dutta, J.; Mala, A. A. Removal of Antibiotic from the Water Environment by the Adsorption Technologies: A Review. *Water Sci. Technol.* **2020**, *82*, 401–426.
- (27) Xu, Y.; Ma, Y.; Ji, H.; Huang, S.; Xie, M.; Zhao, Y.; Xu, H.; Li, H. Enhanced Long-Wavelength Light Utilization with Polyaniline/Bismuth-Rich Bismuth Oxysulfide Composite towards Photocatalytic Degradation of Antibiotics. *J. Colloid Interface Sci.* **2019**, *537*, 101–111.
- (28) Gao, Y.; Li, Y.; Zhang, L.; Huang, H.; Hu, J.; Shah, S. M.; Su, X. Adsorption and Removal of Tetracycline Antibiotics from Aqueous Solution by Graphene Oxide. *J. Colloid Interface Sci.* **2012**, *368*, 540–546.
- (29) Chandak, S.; Ghosh, P. K.; Gogate, P. R. Treatment of Real Pharmaceutical Wastewater Using Different Processes Based on Ultrasound in Combination with Oxidants. *Process Saf. Environ. Prot.* **2020**, *137*, 149–157.
- (30) Miranda, C. D.; Godoy, F. A.; Lee, M. R. Current Status of the Use of Antibiotics and the Antimicrobial Resistance in the Chilean Salmon Farms. *Front. Microbiol.* **2018**, *9*, No. 1284.
- (31) Bojarski, B.; Kot, B.; Witeska, M. Antibacterials in Aquatic Environment and Their Toxicity to Fish. *Pharmaceuticals* **2020**, *13*, No. 189.
- (32) Ozumchelouei, E. J.; Hamidian, A. H.; Zhang, Y.; Yang, M. Physicochemical Properties of Antibiotics: A Review with an Emphasis on Detection in the Aquatic Environment. *Water Environ. Res.* **2020**, *92*, 177–188.
- (33) Bielen, A.; Šimatović, A.; Kosić-Vukšić, J.; Senta, I.; Ahel, M.; Babić, S.; Jurina, T.; González Plaza, J. J.; Milaković, M.; Udiković-Kolić, N. Negative Environmental Impacts of Antibiotic-Contaminated Effluents from Pharmaceutical Industries. *Water Res.* **2017**, *126*, 79–87.
- (34) Managaki, S.; Murata, A.; Takada, H.; Tuyen, B. C.; Chiem, N. H. Distribution of Macrolides, Sulfonamides, and Trimethoprim in Tropical Waters: Ubiquitous Occurrence of Veterinary Antibiotics in the Mekong Delta. *Environ. Sci. Technol.* **2007**, *41*, 8004–8010.
- (35) Yang, J.-F.; Ying, G.-G.; Zhao, J.-L.; Tao, R.; Su, H.-C.; Liu, Y.-S. Spatial and Seasonal Distribution of Selected Antibiotics in Surface Waters of the Pearl Rivers, China. *J. Environ. Sci. Health B* **2011**, *46*, 272–280.
- (36) Zhou, L.-J.; Ying, G.-G.; Zhao, J.-L.; Yang, J.-F.; Wang, L.; Yang, B.; Liu, S. Trends in the Occurrence of Human and Veterinary Antibiotics in the Sediments of the Yellow River, Hai River and Liao River in Northern China. *Environ. Pollut. Barking Essex* **1987** **2011**, *159*, 1877–1885.
- (37) Heberer, T. Occurrence, Fate, and Removal of Pharmaceutical Residues in the Aquatic Environment: A Review of Recent Research Data. *Toxicol. Lett.* **2002**, *131*, 5–17.
- (38) López, J. E.; Builes, S.; Heredia Salgado, M. A.; Tarelho, L. A. C.; Arroyave, C.; Aristizábal, A.; Chavez, E. Adsorption of Cadmium Using Biochars Produced from Agro-Residues. *J. Phys. Chem. C* **2020**, *124*, 14592–14602.
- (39) Saldarriaga, J. F.; Aguado, R.; Pablos, A.; Amutio, M.; Olazar, M.; Bilbao, J. Fast Characterization of Biomass Fuels by Thermogravimetric Analysis (TGA). *Fuel* **2015**, *140*, 744–751.
- (40) Rutherford, D. W.; Wershaw, R. L.; Rostad, C. E.; Kelly, C. N. Effect of Formation Conditions on Biochars: Compositional and Structural Properties of Cellulose, Lignin, and Pine Biochars. *Biomass Bioenergy* **2012**, *46*, 693–701.
- (41) Tan, Z.; Yuan, S.; Hong, M.; Zhang, L.; Huang, Q. Mechanism of Negative Surface Charge Formation on Biochar and Its Effect on the Fixation of Soil Cd. *J. Hazard. Mater.* **2020**, *384*, No. 121370.



- (42) Pintor, A. M. A.; Ferreira, C. I. A.; Pereira, J. C.; Correia, P.; Silva, S. P.; Vilar, V. J. P.; Botelho, C. M. S.; Boaventura, R. A. R. Use of Cork Powder and Granules for the Adsorption of Pollutants: A Review. *Water Res.* **2012**, *46*, 3152–3166.
- (43) Kim, W.-K.; Shim, T.; Kim, Y.-S.; Hyun, S.; Ryu, C.; Park, Y.-K.; Jung, J. Characterization of Cadmium Removal from Aqueous Solution by Biochar Produced from a Giant Miscanthus at Different Pyrolytic Temperatures. *Bioresour. Technol.* **2013**, *138*, 266–270.
- (44) Ahmad, M.; Lee, S. S.; Dou, X.; Mohan, D.; Sung, J.-K.; Yang, J. E.; Ok, Y. S. Effects of Pyrolysis Temperature on Soybean Stover- and Peanut Shell-Derived Biochar Properties and TCE Adsorption in Water. *Bioresour. Technol.* **2012**, *118*, 536–544.
- (45) Chen, Z.; Chen, B.; Zhou, D.; Chen, W. Bisolute Sorption and Thermodynamic Behavior of Organic Pollutants to Biomass-Derived Biochars at Two Pyrolytic Temperatures. *Environ. Sci. Technol.* **2012**, *46*, 12476–12483.
- (46) Li, M.; Liu, Q.; Guo, L.; Zhang, Y.; Lou, Z.; Wang, Y.; Qian, G. Cu(II) Removal from Aqueous Solution by *Spartina Alterniflora* Derived Biochar. *Bioresour. Technol.* **2013**, *141*, 83–88.
- (47) Li, Y.; Zhu, L.; Shi, J.; Dou, Y.; Li, S.; You, R.; Zhang, S.; Miao, X.; Shi, S.; Ji, H.; Yang, G. Super-Hydrophilic Microporous Biochar from Biowaste for Supercapacitor Application. *Appl. Surf. Sci.* **2021**, *561*, No. 150076.
- (48) Amen, R.; Yaseen, M.; Mukhtar, A.; Klemeš, J. J.; Saqib, S.; Ullah, S.; Al-Sehemi, A. G.; Rafiq, S.; Babar, M.; Fatt, C. L.; Ibrahim, M.; Asif, S.; Qureshi, K. S.; Akbar, M. M.; Bokhari, A. Lead and Cadmium Removal from Wastewater Using Eco-Friendly Biochar Adsorbent Derived from Rice Husk, Wheat Straw, and Corn cob. *Clean. Eng. Technol.* **2020**, *1*, No. 100006.
- (49) Chu, J.-H.; Kang, J.-K.; Park, S.-J.; Lee, C.-G. Enhanced Sonocatalytic Degradation of Bisphenol A with a Magnetically Recoverable Biochar Composite Using Rice Husk and Rice Bran as Substrate. *J. Environ. Chem. Eng.* **2021**, *9*, No. 105284.
- (50) Xiong, Q.; Wu, X.; Lv, H.; Liu, S.; Hou, H.; Wu, X. Influence of Rice Husk Addition on Phosphorus Fractions and Heavy Metals Risk of Biochar Derived from Sewage Sludge. *Chemosphere* **2021**, *280*, No. 130566.
- (51) Goh, K.-H.; Lim, T.-T.; Dong, Z. Application of Layered Double Hydroxides for Removal of Oxyanions: A Review. *Water Res.* **2008**, *42*, 1343–1368.
- (52) de Sousa, D. N. R.; Insa, S.; Mozeto, A. A.; Petrovic, M.; Chaves, T. F.; Fadini, P. S. Equilibrium and Kinetic Studies of the Adsorption of Antibiotics from Aqueous Solutions onto Powdered Zeolites. *Chemosphere* **2018**, *205*, 137–146.
- (53) Limousin, G.; Gaudet, J.-P.; Charlet, L.; Sznknect, S.; Barthès, V.; Krimissa, M. Sorption Isotherms: A Review on Physical Bases, Modeling and Measurement. *Appl. Geochem.* **2007**, *22*, 249–275.
- (54) Rath, B. S.; Kumar, P. S. Application of Adsorption Process for Effective Removal of Emerging Contaminants from Water and Wastewater. *Environ. Pollut.* **2021**, *280*, No. 116995.
- (55) Gholamiyan, S.; Hamzehloo, M.; Farrokhnia, A. RSM Optimized Adsorptive Removal of Erythromycin Using Magnetic Activated Carbon: Adsorption Isotherm, Kinetic Modeling and Thermodynamic Studies. *Sustainable Chem. Pharm.* **2020**, *17*, No. 100309.
- (56) Mohamad-Aziz, S. N.; Zularisam, A. W.; Sakinah, A. M. M. Partitioning Isotherm and Kinetic of Erythromycin into Mixed Reverse Micelle during Forward Transfer. *J. Mol. Liq.* **2019**, *288*, No. 111086.
- (57) Foo, K. Y.; Hameed, B. H. Insights into the Modeling of Adsorption Isotherm Systems. *Chem. Eng. J.* **2010**, *156*, 2–10.
- (58) Vieira, F. R.; Romero Luna, C. M.; Arce, G. L. A. F.; Ávila, I. Optimization of Slow Pyrolysis Process Parameters Using a Fixed Bed Reactor for Biochar Yield from Rice Husk. *Biomass Bioenergy* **2020**, *132*, No. 105412.
- (59) Claoston, N.; Samsuri, A. W.; Ahmad Husni, M. H.; Mohd Amran, M. S. Effects of Pyrolysis Temperature on the Physicochemical Properties of Empty Fruit Bunch and Rice Husk Biochars. *Waste Manag. Res.* **2014**, *32*, 331–339.
- (60) Mohammed, Z.; Jeelani, S.; Rangari, V. Low Temperature Plasma Treatment of Rice Husk Derived Hybrid Silica/Carbon Biochar Using Different Gas Sources. *Mater. Lett.* **2021**, *292*, No. 129678.
- (61) Liu, Z.; Delgado-Moreno, L.; Lu, Z.; Zhang, S.; He, Y.; Gu, X.; Chen, Z.; Ye, Q.; Gan, J.; Wang, W. Inhibitory Effects of Dissolved Organic Matter on Erythromycin Bioavailability and Possible Mechanisms. *J. Hazard. Mater.* **2019**, *375*, 255–263.
- (62) Fallah, F.; Zargar, M.; Yousefi, M.; Alam, A. N. Synthesis of the Erythromycin-Conjugated Nanodendrimer and Its Antibacterial Activity. *Eur. J. Pharm. Sci.* **2018**, *123*, 321–326.
- (63) Vendra Singh, S.; Chaturvedi, S.; Dhyan, V. C.; Kasivelu, G. Pyrolysis Temperature Influences the Characteristics of Rice Straw and Husk Biochar and Sorption/Desorption Behaviour of Their Biourea Composite. *Bioresour. Technol.* **2020**, *314*, No. 123674.
- (64) Yu, S.; Park, J.; Kim, M.; Ryu, C.; Park, J. Characterization of Biochar and Byproducts from Slow Pyrolysis of Hinoki Cypress. *Bioresour. Technol. Rep.* **2019**, *6*, 217–222.
- (65) Santamarina, J. C.; Klein, K. A.; Wang, Y. H.; Prencke, E. Specific Surface: Determination and Relevance. *Can. Geotech. J.* **2011**, *39*, 233–241.
- (66) ASTM. *Standard Practice for Determination of Adsorptive Capacity of Activated Carbon by Aqueous Phase Isotherm Technique*; ASTM International, 2020.
- (67) Tran, H. N.; You, S.-J.; Hosseini-Bandegharai, A.; Chao, H.-P. Mistakes and Inconsistencies Regarding Adsorption of Contaminants from Aqueous Solutions: A Critical Review. *Water Res.* **2017**, *120*, 88–116.
- (68) Gupta, V. K.; Fakhri, A.; Agarwal, S.; Sadeghi, N. Synthesis of MnO<sub>2</sub>/Cellulose Fiber Nanocomposites for Rapid Adsorption of Insecticide Compound and Optimization by Response Surface Methodology. *Int. J. Biol. Macromol.* **2017**, *102*, 840–846.
- (69) Samarghandi, M. R.; Al-Musawi, T. J.; Mohseni-Bandpi, A.; Zarrabi, M. Adsorption of Cephalexin from Aqueous Solution Using Natural Zeolite and Zeolite Coated with Manganese Oxide Nanoparticles. *J. Mol. Liq.* **2015**, *211*, 431–441.
- (70) Mahecha-Rivas, J. C.; Fuentes-Ordoñez, E.; Epelde, E.; Saldarriaga, J. F. Aluminum Extraction from a Metallurgical Industry Sludge and Its Application as Adsorbent. *J. Clean. Prod.* **2021**, *310*, No. 127374.